Effect of irradiation of Si^{5+} ion on Fe doped hydroxyapatite

V. Sarath Chandra[1], K. Elayaraja[1], R. V. Suganthi[1], M. I. Ahymah Joshy[1], I. Sulania[2], P. K. Kulriya[2], K. Asokan[2], D. Kanjilal[2], S. Narayana Kalkura[1*]

[1]*Crystal Growth Centre, Anna University, Chennai 600 025, India*
[2] *Inter-University Accelerator Centre, Aruna Asaf Ali Marg, New Delhi 110067, India*

*Corresponding author. Tel. (+91) 44 22358335; E-mail: kalkurasn@annauniv.edu, kalkura@yahoo.com

ABSTRACT

Hydroxyapatite (HAp, $Ca_{10}(PO_4)_6(OH)_2$) is the main inorganic component of hard tissues like bone and teeth. HAp incorporated with magnetic ions, play an important role in cell separation, magnetic resonance imaging (MRI), targeted drug delivery and in hyperthermia treatment of cancer. In this study, the effect of 60 MeV Si^{5+} ion on the hydrothermally synthesized Fe^{3+} doped hydroxyapatite (Fe-HAp, 33 nm) was investigated. At higher fluences, partial amorphization with an increase in the cluster size and surface roughness was observed. Depending on the ion fluence, pores ranging from 300 to 360 nm in size were produced. Irradiated Fe-HAp samples showed enhanced haemocompatibility and bioactivity. The drug (amoxycillin, AMX) loaded irradiated samples exhibited high antimicrobial activity. Copyright © 2013 VBRI press.

Keywords: Irradiation; magnetic material; hyperthermia; bioactivity.

Introduction

Bioceramics are widely used in the fabrication of hip, bone and dental implants. Calcium phosphates are bioceramic materials which could be used as artificial bone substitutes [1-3]. Hydroxyapatite (HAp - $Ca_{10}(PO_4)_6(OH)_2$) is extensively used for hard tissue replacement of bone and teeth, owing to its excellent biocompatibility and bioactivity. The pure HAp has low bonding ability and poor mechanical properties. Hence it could not be used for load bearing applications [4]. The mechanical properties of HAp could be enhanced by the fabrication of composites of HAp and doping with different metal ions [5-7].

Iron is one of the essential trace elements present in bone and teeth [8]. It is a micronutrient essential for various biological processes and is an important component of metalloproteins. In human body, about 60-70 % of iron is present in haemoglobin as circulating erythrocytes. In the intestinal lumen, iron exists as ferrous and ferric salts [9].

The pure phase of HAp has no magnetic properties. Magnetic ion (Fe, Co, Ni, etc.,) incorporated HAp, exhibit strong ferromagnetic properties. Nowadays, magnetic HAp (Fe-HAp) is used for cell separation, targeted drug delivery, magnetic resonance imaging (MRI) and as heat mediator for the hyperthermia treatment of cancer [10]. The crystallinity was found to decrease with an increase in Fe^{2+} concentration on Fe-HAp [8]. Fe^{3+} incorporation, resulted in paramagnetism and an increase in magnetic susceptibility [11, 12]. HAp doped with Fe^{3+}, Cr^{3+} and Zn^{2+} ions have potential applications as active constituents of sunscreens [13]. The *in vivo* cancer hyperthermia study performed using Fe-HAp nanoparticles, exhibited better heating efficacy on tumours, when it was exposed to an external magnetic field [14]. In addition, Fe-HAp showed better bioactivity, haemocompatibillity, osteointegration and were found to be non cytotoxic when compared with pure phase of HAp [12, 15].

Ion beam irradiation (O^+, Si^{++}, Ar^+ and Ag^{7+}) on HAp was found to improve the surface roughness, wettability, mechanical properties, cell adherence and drug loading/release [16-19]. The 1.0 MeV Xe^{2+} ion beam irradiation, amorphized nanocrystalline ZrO_2 [20]. HAp layer was formed on the titanium surface by ion bombardment of Ca^+ and P^+ ion [21]. The irradiation of 30 MeV cluster beams of C_{60} produced tracks on fluorapatite (FAp) [22]. Gamma ray irradiated HAp/poly-L-lactide (PLLA) samples showed significant modification in the surface properties. During irradiation physicochemical changes occurred in the PLLA phase, while the HAp phase remains stable [23]. The swift heavy 100 MeV O^{7+} ion irradiation on HAp enhanced the *in vitro* bioactivity [24]. 125 MeV Si^{9+} ion irradiated HAp thin films showed no cytotoxycity [25]. Here, we report the effect of Si^{5+} ion irradiation on hydrothermally synthesized Fe-HAp. The physical and *in vitro* biological responses of pristine and irradiated samples were investigated.

Experimental

Material Synthesis:

The Fe-HAp powder was synthesized by hydrothermal method using calcium nitrate tetra hydrate [$Ca(NO_3)_2 \cdot 4H_2O$, Merck], diammonium hydrogen phosphate [$(NH_4)_2HPO_4$, Merck], ferric chloride [$FeCl_3$, Qualigens] and ammonia solution (Merck). 0.1 M $FeCl_3$ salt dissolved in 0.5 M of calcium nitrate tetra hydrate solution was prepared using deionized water. This solution was added drop wise into 0.3 M of $(NH_4)_2HPO_4$ solution with vigorous stirring for 2 h at room temperature. During the reaction, the pH of the solution was maintained at 10.5 using ammonia solution. After mixing, the precipitated solution was subjected to the hydrothermal treatment at 170 °C for 6 h and the pressure developed inside the teflon lined chamber was 150 psi. The samples were washed with deionized water and dried at 100 °C in a hot air oven. Fe-HAp pellets of 8 mm diameter and 1 mm thickness were prepared by applying a pressure of 2 tons using hydraulic press was used for irradiation studies.

Irradiation Experiments:

Fe-HAp pellets were irradiated with 60 MeV Si ion with a 5^+ charge state and fluences ranging from 1×10^{11}, 1×10^{12} and 1×10^{13} ions/cm^2 with a current in the range of 1pnA (particles nano Ampere) using 15UD Pelletron Accelarator at IUAC, New Delhi. The samples were mounted on a copper base plate and the beam scan area was 10 mm x 10 mm on the pellet using magnetic scanner. Based on SRIM 2009 (Stopping and Ranging of Ions in Matter) calculation [26], the projected range of the 60 MeV Si^{5+} on Fe-HAp pellets was found to be 14.53 μm. The electronic energy loss (S_e) and nuclear energy loss (S_n) on the samples were 4.122×10^2 eV/Å and 4.115×10^{-1} eV/Å, respectively.

Methods of Characterization:

GXRD was carried out on pristine and irradiated samples using Bruker AXS diffract Plus/D8 advance diffractometer applying maximum power of 30 kV/40 mA with CuKα radiation (λ = 0.154 nm), two theta range of 20-50 ° with scan speed of 1 °/min and step rate 0.02. The glancing angle was fixed at 2 °. The Scherrer equation was used to calculate the crystallite size, $D = K\lambda / \beta \cos\theta$ where, K is the shape factor (0.9), β is the broadening of the full width at half maximum (FWHM) of the diffraction peak measured in radians, λ is the wavelength of the X-rays and θ is the Bragg's diffraction angle [27]. The crystallinity (X_c) was determined by an empirical relation between X_c and $\beta_{(002)}$ ie. $\beta_{(002)} \times \sqrt[3]{X_c} = K_A$ where, $\beta_{(002)}$ is FWHM of (002) in degree and K_A is a constant (0.24). The lattice parameters and crystal structure were obtained by using the Rietveld refining of the XRD pattern on Material Analysis Using Diffraction (MAUD) crystallographic computation program [28]. The surface morphology of pristine and irradiated samples was studied using multimode atomic force microscope (AFM) and magnetic force microscope (MFM) using Digital Instruments Nanoscope IIIa SPM by tapping mode at room temperature. The particle size, porosity and surface roughness were analyzed from the area of X and Y axis of 5×5 μm^2 surface (AFM) topography with the help of Nanoscope software. MFM measurements were performed at different lift heights before and after irradiation without any applied magnetic field. An antimony doped silicon tip coated with magnetic layer of Co/Cr was used. Bioactivity tests were carried out by immersing the samples in simulated body fluid (SBF). The SBF solution was prepared by dissolving the reagent grade chemicals of KCl, $K_2HPO_4 \cdot 3H_2O$, $MgCl_2 \cdot 6H_2O$, 1M HCl, $CaCl_2 \cdot 2H_2O$, Na_2SO_4 and $((HOCH_2)_3CNH_2)$ (TRIS) in deionized water and buffered to pH 7.4 at 37 ± 0.1 °C with HCl [29]. The initial weight was weighed (W_1) for all the samples. Then the pellet was immersed in 15 mL of SBF in an air tight plastic container. The solution was renewed once in two days, and after four weeks the pellets were taken out from the SBF solution and allowed to air dry at 37 ± 0.1 °C. The pellets were reweighed (W_2). The surface morphology of the samples was observed by scanning electron microscope (SEM, LEO 440 STEREOSCAN, Leica).

Acid Citrate Dextrose (ACD) human blood was used to study the blood compatibility by haemolytic assay. ACD solution was prepared by mixing 0.544 gm of anhydrous citric acid, 1.65 gm of trisodium citrate dihydrate and 1.84 gm of dextrose monohydrate. ACD blood was prepared by adding 1 mL of ACD solution to 9 mL of fresh human blood. Initially, the pellets of 0.05 gm were sterilized under UV for 1 h for sterilization. The sterilized pellets were equilibrated with 1 mL of saline for about 24 h in sterile centrifuge tubes at 37 °C in an incubator subsequently the saline was removed and 0.25 mL of ACD blood was added and incubated for 20 min. Afterward, 2 mL of sterile saline was added to stop haemolysis and were incubated for 1 h then the pellets were spun at 750G for 5 min. Human blood with deionized water served as the positive control and sterile saline served as the negative control. The supernatants were transferred into a quartz cuvette and the absorbance in the assay was measured using UV spectrophotometer (UV-1601, Shimadzu) at 545 nm. Percentage of haemolysis is calculated using the formula, Percentage of haemolysis = {(OD for the Test Sample − OD for the −ve Control) / (OD for the +ve Control − OD for the −ve Control)}. The calculated percentage of haemolysis for all the samples were compared with ASTM standard, Highly Haemocompatible - <5 % Haemolysis, Haemocompatible within 10 % Haemolysis and Non Haemocompatible - >20 % Haemolysis.

The drug loading experiment was performed by dissolving 50 mg of amoxycillin (AMX) drug in 1.0 mL of deionized water. The irradiated samples were immersed into drug solution and it was kept at 27 °C with a shaking speed of 100 rpm using incubator-cum-orbital shaker for 24 h. The antimicrobial activity was carried out using agar diffusion test. Muller-Hinton agar (MHA, Merck) was used as a base medium and nutrient broth was used for the preparation of inoculum. A sterile cotton swab was dipped into the standardized bacterial culture of *S. aureus* containing the cell of 1×10^6 CFU/mL. The drug loaded irradiated surface was kept on the agar plate against *S. aureus*. 300 μL of bacterial suspensions of *S. aureus* were spread uniformly on the agar plate. These cells were inoculated on the entire surface of the MHA plate and allowed for 10 min at the room temperature. The plates

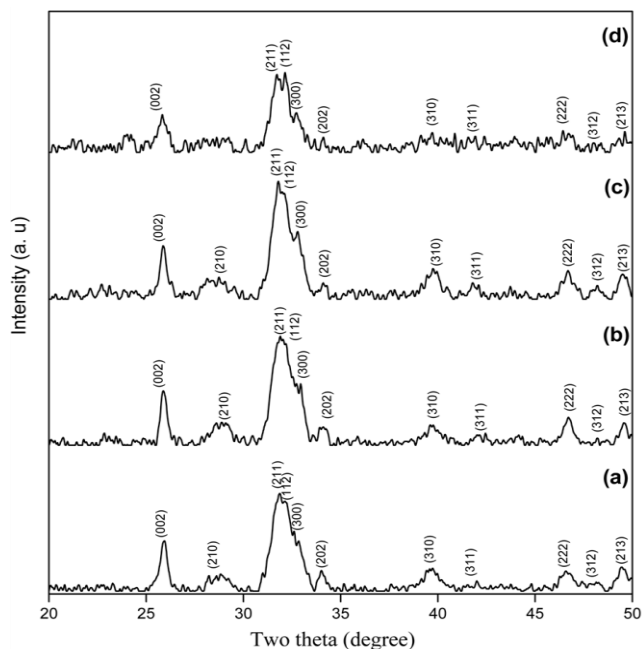were incubated at 37 ºC for 24 h and the zone of inhibition was recorded.

Fig. 1. GXRD patterns of (a) Pristine, (b) 1×10^{11}, (c) 1×10^{12} and (d) 1×10^{13} ions/cm^2 irradiated samples.

Table 1. Lattice parameters, Crystallite size and Crystallinity of (002) plane of pristine and irradiated samples.

Samples	Lattice Parameters (Å) a (± 0.02)	Lattice Parameters (Å) c (± 0.01)	Crystallite Size (D) (± 1 nm)	Crystallinity (%) (X_c) (± 0.1)
Pristine	9.45	6.86	33	95
Si^{5+} 1 x 10^{11} ions/cm^2	9.44	6.86	32	94
Si^{5+} 1 x 10^{12} ions/cm^2	9.43	6.85	23	84
Si^{5+} 1 x 10^{13} ions/cm^2	9.42	6.84	13	72

Results and discussion

GXRD analysis

The XRD patterns of pristine and Si^{5+} ion irradiated samples were as shown in **Fig. 1 (a-d)**. The XRD patterns were in good agreement with the standard JCPDS data (09-0432) for the pure phase of HAp. The irradiated samples revealed no secondary phases other than that of HAp. The peak intensity was not affected significantly for 1 x 10^{11} ions/cm^2 irradiated samples compared with pristine. Further, there was gradual reduction in the peak intensity at higher fluences (1 x 10^{12} and 1 x 10^{13} ions/cm^2) on irradiation. This may be due to defects created by the SHI in the Fe-HAp lattice **[30, 31]**. The crystallite size, crystallinity and lattice parameters were calculated from XRD patterns. The average crystallite size, crystallinity and

lattice parameters gradually decreased with an increase in ion fluence as shown in **Table 1**.
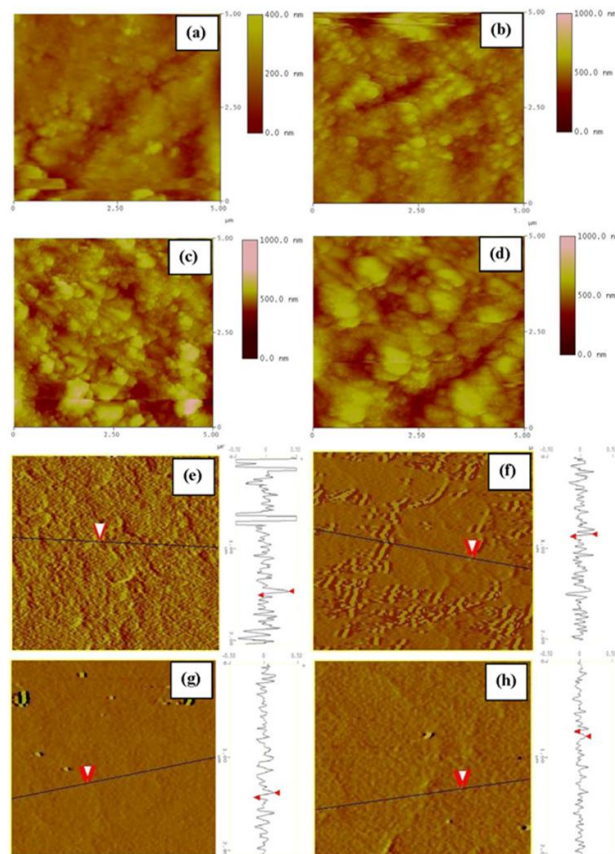

Fig. 2. (a-d) AFM micrographs of (a) Pristine, (b) 1×10^{11}, (c) 1×10^{12} and (d) 1×10^{13} ions/cm^2 irradiated samples. (e-h) MFM micrographs of (e) Pristine, (f) 1×10^{11}, (g) 1×10^{12} and (h) 1×10^{13} ions/cm^2 irradiated samples.

Table 2. AFM/MFM results of pristine and irradiated samples.

Sample	Average size of cluster (± 1 nm)	AFM Roughness (RMS) (± 1 nm)	Pores size (± 1 nm)	MFM Phase shift ($\pm 0.05°$)
Pristine	253	52	-	0.40
Si^{5+} 1 x 10^{11} ions/cm^2	273	58	300	0.33
Si^{5+} 1 x 10^{12} ions/cm^2	292	67	351	0.29
Si^{5+} 1 x 10^{13} ions/cm^2	673	76	360	0.16

AFM analysis

AFM surface micrograph images of the pristine and irradiated samples were as shown in **Fig. 2 (a-d)**. The pristine samples showed smooth surface **(Fig. 2a)**, whereas irradiated samples surface was very rough **(Fig. 2 b-d)**. The cluster size and surface roughness increased with an increase in ion fluences **(Table 2)**. In the case of 1×10^{11} and 1×10^{12} ions/cm^2 irradiated samples, hillock structures were formed on the surface **(Fig. 2b, 2c)**. At higher fluence (1×10^{13} ions/cm^2) the surface revealed large clusters with high roughness. This may be due to the thermal spike effect; the phenomena in the case of ion-irradiation such as

energetic atoms fall on the material above melting point, it causes local heat due to electron-ion interaction. This melting was followed by a rapid quenching, leading to the formation of larger grains or clusters on the sample surface [25, 32]. The pores of 300 to 360 ± 1 nm were produced by local heating due to the electronic energy loss on the irradiated samples [33] (**Table 2**).
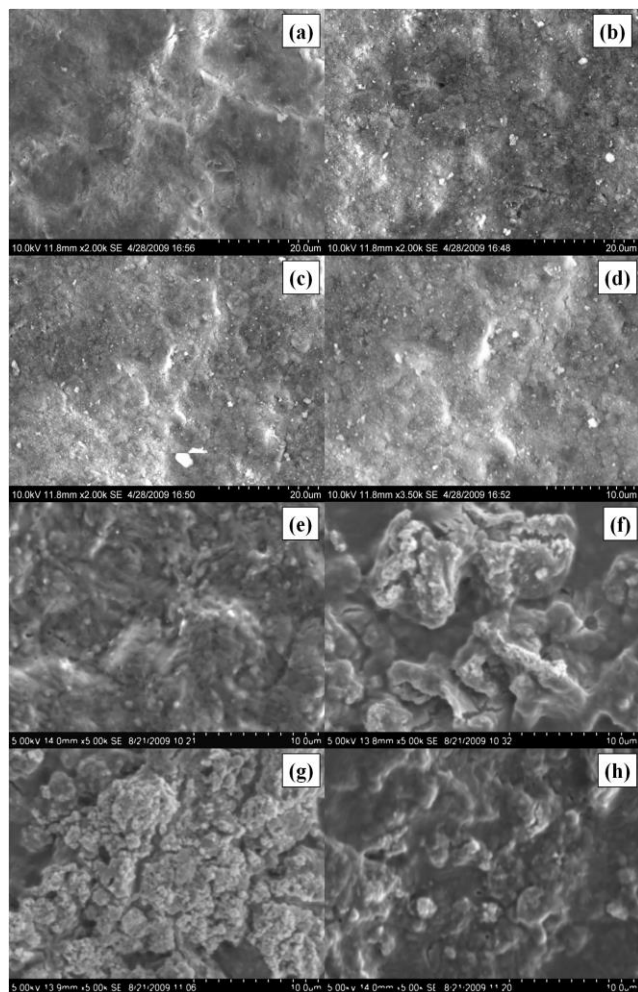

Fig. 3. SEM photographs of the unsoaked (a) Pristine, (b) $1x10^{11}$, (c) $1x10^{12}$ and (d) $1x10^{13}$ ions/cm^2 and SBF soaked samples (e) Pristine, (f) $1x10^{11}$, (g) $1x10^{12}$ and (h) $1x10^{13}$ ions/cm^2.

The magnetic domain structures of pristine and irradiated samples were as shown in **Fig. 2 (e-h)**. The phase images were studied at different lift heights and the lift height for MFM measurement was kept at 30 nm after ensuring that the phase image does not have contribution from topographic features. The observed MFM image could be characterized by darker regions adjacent to the bright regions in the nanometer scale and the magnetic regions seems to be distributed uniformly along the plane of the Fe-HAp matrix. The average contrast between dark and bright area is measured by means of section analysis. From the analysis of the MFM data, we have calculated the corresponding root mean square (RMS) phase shift of the pristine/irradiated samples. The value of phase shift was found to be 0.40° for pristine and for the irradiated samples it decreased from 0.33° to 0.17° with an increase in ion fluence.

Table 3. Change in weight before and after SBF soaked samples.

Sample	Before Soaking (mg)	After Soaking (mg)
Pristine	92.41	97.89
Si^{5+} 1 x 10^{11} ions/cm^2	83.39	88.88
Si^{5+} 1 x 10^{12} ions/cm^2	87.85	93.55
Si^{5+} 1 x 10^{13} ions/cm^2	79.95	85.38

In vitro bioactivity test

The SEM micrographs of the unsoaked samples are as shown in **Fig. 3 (a-d)**. The pristine sample surface exhibited (**Fig. 3a**) smooth surface, whereas cluster like morphology were observed with an increase in ion fluences **Fig. 3 (b-d)**. The bone bonding ability of a material depends on its apatite inducing ability when immersed in SBF- a synthetically prepared fluid whose ion concentration is nearly equal to that of human blood plasma. On immersion in SBF, the pristine sample showed deposition of apatite layer through out the surface with pores and spheroids of size 2-3 μm (**Fig. 3e**). The cluster of spheroids was observed on irradiated samples surface (**Fig. 3f, 3h**). The irradiated samples showed increase in apatite growth on the surface, with increase in ion fluence, which was further confirmed by the weight difference between initial and final weight of the samples (**Table 3**). The surface of the pristine and irradiated samples reveals more negative surface charge due to phosphate (PO_4^{3-}) and hydroxyl (OH^-) ions. These negative ions interact with the positive calcium ions in the SBF to form Ca-rich apatite (amorphous calcium phosphate) on the irradiated Fe-HAp surface which gain positive surface charge. The Ca-rich ACP interacts with the negative phosphate ions in the SBF to form the Ca-poor ACP, which stabilizes by being crystallized into bone like apatite in the SBF [34 - 36].
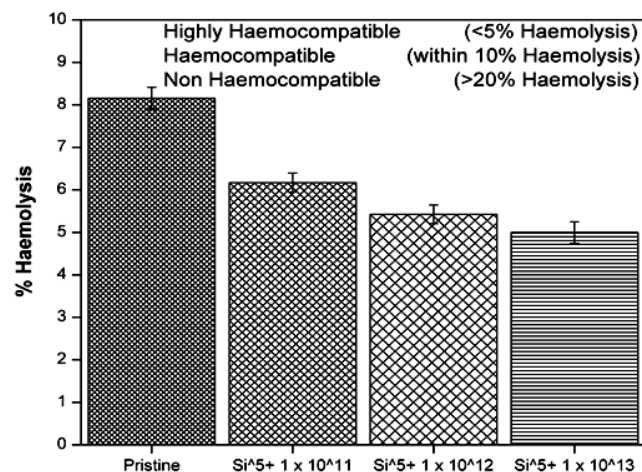

Fig. 4. Haemolytic assay of (a) Pristine, (b) $1x10^{11}$, (c) $1x10^{12}$ and (d) $1x10^{13}$ ions/cm^2 irradiated samples.

Haemolysis assay

The percentage of haemolysis for the pristine and irradiated samples was as shown in **Fig. 4**. The none of the samples caused haemolysis. The percentage of haemolysis of pristine and irradiated samples was less than 10%, which was within the acceptable limit as per the ASTM standards **[37]**. These studies revealed that the irradiation of Fe^{3+} did not affect the biocompatibility of the samples.

Antimicrobial activity

The antibacterial activity of AMX free and loaded pristine and irradiated samples was determined by agar diffusion test against gram positive bacteria (*S. aureus*) as shown in **Fig. 5 (a-d)**. Drug free pristine and irradiated samples showed no inhibition zone against *S. aureus*. Whereas, AMX loaded pristine and irradiated samples inhibited bacterial growth of *S. aureus* (**Table 4**). In addition, the irradiated samples showed gradual increase in the diameter of inhibition zone, indicating the enhanced drug release from the irradiated samples. The presence of pores, increase in surface roughness and wettability due to irradiation would have led to an increased absorption of drugs and their subsequent release **[25]**.
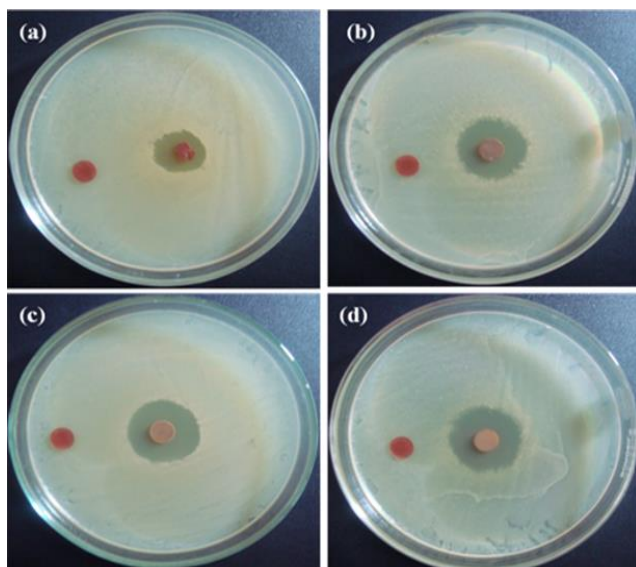
Fig. 5. Agar diffusion test of (a) Pristine, (b) $1x10^{11}$, (c) $1x10^{12}$ and (d) $1x10^{13}$ ions/cm^2 irradiated samples.

Table 4. The zone of inhibition of the antibacterial efficacy against *S. aureus* for the pristine and irradiated samples

Bacterial strain	Sample	Diameter of inhibition zone ($\pm$ 0.5 mm)
S. aureus	Pristine	0.7
	Si^{5+} 1 x 10^{11} ions/cm^2	1.0
	Si^{5+} 1 x 10^{12} ions/cm^2	1.2
	Si^{5+} 1 x 10^{13} ions/cm^2	1.3

Conclusion

The effect of swift heavy Si^{5+} ion (60 MeV) irradiation on Fe-HAp synthesized by hydrothermal technique was investigated. The crystallite size, crystallinity and the lattice parameters decreased with an increase in ion fluences, whereas surface roughness and porosity of the samples were increased on irradiation. The presence of pores assists the flow of the blood fluid into implants which enhances biocompatibility. In addition, the irradiation led to an increase in the haemocompatibility and bioactivity. The Fe-HAp irradiated samples showed better efficacy against *S. aureus* which could help in the treatment of bone and joint infections (osteomyelitis).

Reference

1. Adamopoulos, O.; Papadopoulos, T. *J Mater Sci: Mater Med.* **2007**, 18, 1587.
   DOI: 10.1007/s10856-007-3041-6
2. Vallet-Regi, M.; González-calbet, J. M. *Prog. Solid State Chem.* **2004**, 32, (1-2) 1.
   DOI: 10.1016/j.progsolidstchem.2004.07.001
3. KomLev, V. S.; Barinov, S. M.; Koplik, E. V. *Biomaterials* **2002**, 23, 3449.
   DOI: 10.1016/S0142-9612(02)00049-2
4. Egorov, A. A.; Smirnov, V. V.; Shvorneva, L. I.; Kutsev, S. V.; Barinov, S. M. *Inorg. Mater.* **2010**, 46, 208.
   DOI: 10.1134/S0020168510020147
5. Nathanael, A. J.; Mangalaraj, D.; Hong, S. I.; Masuda, Y. *Mater. Charact.* **2011**, 62, 1109.
   DOI: 10.1016/j.matchar.2011.09.008
6. Inuzuka, M.; Nakamura, S.; Kishi, S.; Yoshida, K.; Hashimoto, K.; Toda, Y.; Yamashita, K. *Solid State Ionics* **2004**, 172, 509.
   DOI: 10.1016/j.ssi.2004.01.054
7. Joshy, M. I. A.; Elayaraja, K.; Suganthi, R. V.; Veerla, S. C.; Kalkura, S. N. *Curr. Appl Phys.* **2011**, 11, 1100.
   DOI: 10.1016/j.cap.2011.02.003
8. Morrissey, R.; Rodriguez-Lorenzo, L. M.; Gross, K. A. *J. Mater. Sci. –Mater. Med.* **2005**, 16, 387.
   DOI: 10.1007/s10856-005-6976-5
9. Lieu, P. T.; Heiskala, M.; Peterson, P. A.; Yang, Y. *Mol. Aspects Med.* **2001**, 22, 1.
   DOI: 10.1016/S0098-2997(00)00006-6
10. Stojanovic, Z.; Veselinovic, L.; Markovic, S.; Ignjatovic, N.; Uskokovic, D. *Mater. Manuf. Processes* **2009**, 24, 1096.
    DOI: 10.1080/10426910903032113
11. Wu, H. C.; Wang, T. W.; Sun, J. S.; Wang, W. H.; Lin, F. H. *Nanotechnology* **2007**, 18.
    DOI: 10.1088/0957-4484/18/16/165601
12. Sarath Chandra, V.; Baskar, G.; Suganthi, R. V.; Elayaraja, K.; Joshy, M. I. A.; Beaula, W. S.; Mythili, R.; Venkatraman, G.; Kalkura, S. N. *ACS Appl. Mater. Interfaces*. **2012**, 4, 1200.
    DOI: 10.1021/am300140q
13. de Araujo, T. S.; de Souza, S. O.; de Sousa, E. M. B. *J. Phys. Conf. Ser.* **2010**, 249, 012012.
    DOI: 10.1088/1742-6596/249/1/012012
14. Hou, C.; Hou, S.; Hsueh, Y.; Lin, J.; Wu, H.; Lin, F. *Biomaterial* **2009**, 30, 3956.
    DOI: 10.1016/j.biomaterials.2009.04.02
15. Li, Y.; Nam, C. T.; Ooi, C. P. *J. Phys. Conf. Ser.* **2007**, 187, 012024.
    DOI: 10.1088/1742-6596/187/1/012024
16. Ananda Sagari, A. R.; Rahkila, P.; Väisänen, M.; Rehto, R.; Sajavaara, T.; Gorelick, S.; Laitinen, M.; Putkonen, M.; Sangyuenyongpipat, S.; Timonen, J.; Cheng, S.; Whitlow, H. J. *Nucl. Instrum. Methods Phys. Res., Sect. B.* **2008**, 266, 2515.
    DOI: 10.1016/j.nimb.2008.03.069

17. Lopatin, C. M.; Alford, T. L.; Pizziconi, V. B.; Kuan, M.; Laursen, T. *Nucl. Instrum. Methods Phys. Res., Sect. B.* **1998**, 145, 522.
    DOI: 10.1016/S0168-583X(98)80557-0

18. Nelea, V.; Pelletier, H.; Müller, D.; Broll, N.; Mille, P.; Ristoscu, C.; Mihailescu, L. N. *Appl. Surf. Sci.* **2002**, 186, 483.
    DOI: 10.1016/j.matchemphys.2012.03.018

19. Elayaraja, K.; Rajesh, P.; Joshy, M. I. A.; Sarath Chandra, V.; Suganthi, R. V.; Kennedy, J.; Kulriya, P. K.; Sulania, I.; Asokan, K.; Kanjilal, D.; Avasthi, D. K.; Varma, H. K.; Kalkura, S. N. *Mater. Chem. Phys.* **2012**, 134, 464.
    DOI: 10.1016/S0168-583X(03)00519-6

20. Meldrum, A.; Boatner, L. A.; Ewing, R. C. *Nucl. Instrum. Methods Phys. Res., Sect. B.* **2003**, 207, 28.
    DOI: 10.1016/S0168-583X(03)00519-6

21. Rautray, T. R.; Narayanan, R.; Kwon, T.; Kim, K. *Thin Solid Films* **2010**, 518, 3160.
    DOI: 10.1016/j.tsf.2009.08.044

22. Jaskierowicz, G.; Dunlop, A.; Jonckheere, R. *Nucl. Instrum. Methods Phys. Res., Sect. B.* **2004**, 222, 213.
    DOI: 10.1016/j.nimb.2004.01.224

23. Suljovrujić, E.; Ignjatović, N.; Uskoković, D. *Radiat. Phys. Chem.* **2003**, 67, 375.
    DOI: 10.1016/S0969-806X(03)00070-7

24. Girija, E. K.; Parthiban, S. P.; Suganthi, R. V.; Elayaraja, K.; Joshy, M. I. A.; Vani, R.; Kularia, P.; Asokan, K.; Kanjilal, D.; Yokogawa, Y.; Kalkura, S. N. *J. Ceram. Soc. Jpn.* **2008**, 116, 320.
    DOI: 10.2109/jcersj2.116.320

25. Elayaraja, K.; Joshy, M. I. A.; Suganthi, R. V.; Kalkura, S. N.; Palanichamy, M.; Ashok, M.; Sivakumar, V. V.; Kulriya, P. K.; Sulania, I.; Kanjilal, D.; Asokan, K. *Appl. Surf. Sci.* **2011**, 257, 2134.
    DOI: 10.1016/j.apsusc.2010.09.062

26. SRIM and TRIM software, http://www.srim.org.

27. Klug, H. P.; Alexander, L. E. In: X-ray Diffraction Procedures for Polycrystalline and Amorphous Materials, second ed. Willey, Newyork, **1947**.

28. Lutterotti L.; Scardi, P. *J. Appl. Crystallogr.* **1990**, 23, 246.
    DOI: 10.1107/S0021889890002382

29. Kokubo, T.; Takadama, H. *Biomaterials* **2006**, 27, 2907.
    DOI: 10.1016/j.biomaterials.2006.01.017

30. Nagabhushana, K. R.; Lakshminarasappa, B. N.; Pandurangappa, C.; Sulania, I.; Kulria, P. K.; Singh. F. *Nucl. Instrum. Methods Phys. Res., Sect. B.* **2008**, 266, 1475.
    DOI: 10.1016/j.nimb.2008.01.036

31. Mene, R. U.; Mahabole, M. P.; Sharma, R.; Khairnar, R. S. *Vacuum* **2011**, 86, 66.
    DOI: 10.1016/j.vacuum.2011.04.015

32. Mene, R. U. ; Mahabole, M. P. ; Khairnar, R. S. ; *Radiat. Phys. Chem.* **2011**, 80, 682.
    DOI: 10.1016/j.radphyschem.2011.02.002

33. Fleischer, R. L.; Price, P. B.; Walker, R. M. *J. Appl. Phys.* **1965**, 36, 3645.
    DOI: 10.1063/1.1703059

34. Parthiban, S. P.; Suganthi, R.V.; Girija, E. K.; Elayaraja, K.; Kulriya, P. K.; Katharria, Y. S.; Singh, F.; Sulania, I.; Tripathi, A.; Asokan, K.; Kanjilal, D.; Yadav, S.; Singh, T. P.; Yokogawa, Y.; Kalkura, S. N. *Nucl. Instrum. Methods Phys. Res., Sect. B.* **2008**, 266, 911.
    DOI: 10.1016/j.nimb.2008.02.026

35. Kim, H.; Himeno, T.; Kawashita, M.; Kokubo, T.; Nakamura, T. *J. R. Soc. Interface* **2004**, 1, 17.
    DOI: 10.1098/rsif.2004.000

36. Suganthi, R. V.; Parthiban, S. P.; Elayaraja, K.; Girija, E. K.; Kulariya, P.; Katharria, Y. S.; Singh, F.; Asokan, K.; Kanjilal, D.; Kalkura, S. N. *J Mater Sci: Mater Med.* **2009**, 20, S271.
    DOI: 10.1007/s10856-008-3652-6

37. Chowdhury, S. K. R.; Mishra, A.; Pradhan, B.; Saha, D. *Wear* **2004**, 256, 1026.
    DOI: 10.1016/S0043-1648(03)00535-0